Geophysical Research Letters

RESEARCH LETTER
10.1029/2025GL115483

Field-Aligned Proton Beams Upstream of the Martian Bow Shock: First Observations

K. Meziane[1], C. X. Mazelle[2], C. Simon-Wedlund[3], J. S. Halekas[4], A. M. Hamza[1], C. Bertucci[5], D. L. Mitchell[6], and J. R. Espley[7]

[1]Physics Department, University of New Brunswick, Fredericton, NB, Canada, [2]IRAP, CNRS, UPS, CNES, Université de Toulouse, Toulouse, France, [3]Space Research Institute, Austrian Academy of Sciences, Graz, Austria, [4]Department of Physics and Astronomy, University of Iowa, Iowa City, IA, USA, [5]IAFE, UBA CONICET, Buenos Aires, Argentina, [6]Space Sciences Laboratory, University of California, Berkeley, Berkeley, CA, USA, [7]NASA Goddard Space Center, Greenbelt, MD, USA

Key Points:

- First evidence of backstreaming proton field-aligned beams upstream of the Martian bow shock
- The beams can be seen along field lines that connect the quasi-parallel shock
- The beams closely resemble those in the terrestrial foreshock

Supporting Information:

Supporting Information may be found in the online version of this article.

Correspondence to:

K. Meziane,
karim@unb.ca

Citation:

Meziane, K., Mazelle, C. X., Simon-Wedlund, C., Halekas, J. S., Hamza, A. M., Bertucci, C., et al. (2025). Field-aligned proton beams upstream of the Martian bow shock: First observations. *Geophysical Research Letters*, *52*, e2025GL115483. https://doi.org/10.1029/2025GL115483

Received 23 FEB 2025
Accepted 24 MAR 2025

Abstract We report fast sunward-propagating energetic proton field-aligned beams (FABs) observed about one Mars radius upstream of the Martian bow shock, recorded by the Solar Wind Ion Analyzer instrument on the MAVEN spacecraft. The velocity distributions show that all the beams have a bulk parallel speed $v_B = (1.35 \pm 0.21)V_S$, exceeding the shock speed V_S. Several FABs are observed in the field-aligned region, linked to the quasi-parallel shock. The nearly synchronous variations of shock θ_{Bn} values and beam speeds rule out specular reflection, suggesting a non-specular reflection mechanism. However, the slower Martian foreshock beam speeds remain unexplained compared to their terrestrial counterparts.

Plain Language Summary On 22 September 2014, the MAVEN probe was put into orbit around Mars, with the primary mission focussed on studying the Martian neutral gas and plasma environment. The primary goal of this research includes examining interactions with the solar wind—plasma emanating from the Sun—and solar radiation. As the solar wind encounters Mars, it is disrupted by the planet, which acts as an obstacle. creating a shock wave just upstream. This shock wave energizes a small portion of the solar wind protons, causing them to be reflected toward space instead of continuing around the planet. For the first time, we present a detailed study of this backstreaming population at Mars and compare its properties to those observed in Earth's environment.

1. Introduction

Standing foreshocks arise when a planetary shock develops. While a shock is caused by the interaction of the solar wind with the planetary obstacle, the resulting foreshock corresponds to the space region upstream of the shock in which the upstream interplanetary magnetic field (IMF) lines are connected to the shock surface. The terrestrial foreshock has been the focal point of many extensive investigations. However, satellite missions to various planets in the solar system have enabled the collection of in situ data, which in turn has allowed scientists to shift their attention away from the terrestrial foreshock and focus on various planetary environments in the solar system.

Interacting particles and fields populate the foreshocks, and their physical characteristics are strongly coupled to the spatial location in the foreshock. Both sunward flowing electrons and a broad class of ion velocity distributions populate the region upstream of the bow shock (Thomsen, 1985). Our present interest is on ions collimated along the IMF (also called Field-Aligned Beam or FAB) that appear, in the case of the Earth, to emanate from a region defined by $30° < \theta_{Bn} < 70°$, where θ_{Bn} is the angle that the IMF makes with the local shock normal (Bonifazi & Moreno, 1981).

The plasma environment at Mars differs significantly from that of Earth (Mazelle et al., 2004). Due to Mars' weaker gravity, its exosphere extends beyond the bow shock. Additionally, the absence of a global magnetic field results in a much closer location of the bow shock to the Martian surface, compared to Earth's. Upstream of the bow shock, pick-up ions form the second most abundant ion population after the solar wind. These ions are continuously produced through photoionization, charge exchange, and electron impact ionization at every location in the Martian environment. The question of whether backstreaming ions exist far upstream of the Martian bow shock remains to be explored.

Studies of Mars' foreshock phenomena began with the Phobos-2 mission. Early evidence for ion beams propagating sunward upstream of Mars' bow shock was detected by the ASPERA mass spectrometer, which observed the ion beams when the IMF lines appeared magnetically connected to the shock (Barabash & Lundin, 1993). However, ASPERA could only measure the distribution in the ecliptic plane, and the time required to acquire a full distribution was several times greater than the gyro-period. With the Mars Express (MEX) mission, the identification of field-aligned ion beams became more challenging due to the lack of magnetic field vector measurements. However, evidence for the presence of proton ring-beam distributions upstream of the bow shock have been indirectly inferred (Yamauchi et al., 2012). Using MAVEN data and studying the impact of foreshock transient structures on the Martian bow shock, Madanian et al. (2023) reported velocity distributions associated with suprathermal protons moving sunward. These are seen inside a foreshock bubble and seem to emanate from the quasi-parallel bow shock.

Previous studies of Martian foreshock ions have been primarily qualitative. To our knowledge, no prior observations have directly identified FABs in the Martian foreshock. A quantitative investigation is therefore crucial to better understand the physical mechanisms involved, particularly the generation of FABs at Mars. Furthermore, exploring the source region of these ions at the shock is vital to understanding the Martian ion foreshock and identifying any similarities to the terrestrial ion foreshock. For the first time, ion velocity distribution functions are measured by the MAVEN spacecraft, which carries state-of-the-art instrumentation with high-bit telemetry rates, enabling detailed analysis.

In the following section, we briefly describe the instrumentation used in the present report and the observations are presented. A quantitative characterization as well as a possible production mechanism are developed in Section 3. Finally, a concise discussion is given in the last section.

2. Observations

2.1. Instrumentation

The present work is based on observations from the MAVEN spacecraft, which is currently in orbit around Mars (Jakosky et al., 2015). The data from the Solar Wind Ion Analyzer (SWIA) are of particular interest in this study. This analyzer measures energies per charge in the range of 25 eV/q - 25 keV/q, and allows for a complete reconstruction of the ion velocity distribution function over a time period that depends on the operation mode (Halekas et al., 2015). For solar wind plasma measurements, the Fine Archive mode (SWIFA) provides a distribution every 4 s with a 45° × 45° field of view (FOV) and an angular resolution of 4.5° (Halekas et al., 2015). In contrast, the Coarse Archive mode (SWICA), which is better suited for suprathermal ion measurements, has a broader FOV is 360° × 90°. Although a full angular distribution is collected every 4 s, the time frame for the transmission of snapshots depends on the telemetry mode. For the present study, one full distribution is transmitted only every 32 s. Our study also use magnetic field data from MAG sensors (Connerney et al., 2015) and electron measurements from the Solar Wind Electron Analyzer SWEA instrument (Mitchell et al., 2016).

2.2. Pick up Ion Population

The present work is based on measurements collected by MAVEN on 10 February 2015 during two time intervals from 06:30 UT to 07:45 UT and from 02:25 UT to 04:00 UT. For the first time interval, the corresponding MAVEN's orbit is shown in Figure S1 in Supporting Information S1.

Pickup ions are expected to be ubiquitous around Mars and in particular on the dayside upstream from the bow shock given the planet's extended exosphere well beyond this boundary. In the upstream region, where neutral hydrogen strongly predominates, protons are anticipated to constitute the bulk of the pickup population. Inside the foreshock, the ion population consists of a mixture of solar wind ions, shock-reflected ions, and pickup ions, all of which must be differentiated.

In the solar wind reference frame, the instantaneous velocity **v** of a newly born ion following the ionization of the exospheric neutral atom, is described by the following equation:

$$m\frac{d\mathbf{v}}{dt} = e\mathbf{v}\times\mathbf{B} \tag{1}$$

$$\mathbf{v}(t=0) = -\mathbf{V_{SW}} \quad (2)$$

where m is the pick-up ion mass, e the elementary electric charge ($e > 0$), $\mathbf{B}$ the magnetic field, and $\mathbf{V_{SW}}$ the solar wind velocity. The initial condition given in Equation 2 assumes that the energy gained by the newly born ion via photo-ionization is neglected. From the trivial solution to the above equation, it follows that the newly formed ion acquires instantaneously in the plasma rest frame an initial energy of $(1/2)mV_{SW}^2$ and a pitch-angle $\alpha_P = \pi - \theta_{BV}$, where θ_{BV} is the angle between the magnetic field and the solar wind velocity. In the shock frame of reference, the newborn ions experience the $\boldsymbol{E} \times \boldsymbol{B}$ drift while gyrating about the magnetic field direction. The maximum kinetic energy attained is four times greater that of a similar ion moving under the $|\boldsymbol{E} \times \boldsymbol{B}|$ drift (Jarvinen & Kallio, 2014).

Initially, the velocity distribution of pickup ions is expected to show coherent features, as the ions have not yet scattered in energy and pitch angle on longer characteristic time scales (Yoon et al., 1991). However, at the early stage of their production, both the ion energy and pitch angle provide a clear signature that characterizes the solar wind environment.

The time series of proton pitch-angle spectrogram for four selected energy ranges is shown in Figure 1 undertaken by MAVEN/SWIA on 10 February 2015 between 06:30 UT and 07:45 UT. The pitch angle values are shown in the solar wind rest frame of reference. In other words, the pitch angles are obtained from the velocity components after being converted into the solar wind frame of reference while the phase space density remains an invariant under the Galilean transformation. The two bottom panels display the solar wind velocity and magnetic field components in the Mars-centered Solar Orbital system of coordinates. At the same time, the angle α_p, obtained from SWIA and MAG data, is superposed in black trace in the four panels which present the pitch angle distribution corresponding to the $\sim 4.41-5.10$ keV, $\sim 2.47-2.85$ keV, $\sim 0.90-1.04$ keV, and $\sim 0.67-0.78$ keV energy ranges, respectively.

Clearly, both the spectrograms corresponding to $\sim 0.90-1.04$ keV and $\sim 0.67-0.78$ keV energy ranges exhibit a stripe during the entire time interval corresponding to enhanced numerical values in the distribution function values. A maximum is seen for $\sim 0.67-0.78$ keV ions matching the observed solar wind bulk energy ($V_{SW} \sim 360$ km/s). Newly picked up ion density is expected to be highest at the solar wind bulk energy $\left(\sim(1/2)mV_{SW}^2\right)$ while they concentrate around a pitch angle α_P. The third and fourth panels from the top of Figure 1 clearly show how the time series of the $\alpha_p = \pi - \theta_{BV}$ angle tracks the maximum of the ion distribution. With a lesser intensity due to a smaller pickup ion density, a similar feature is illustrated at higher energy (top 2 panels). One should mention, the presence of low frequency magnetic field fluctuations during the entire interval. These fluctuations point to proton cyclotron waves that are frequently present around the Mars planetary environment and are generated by the newly picked-up protons (Delva et al., 2011).

2.3. FAB Population

In addition to pickup ions, Figure 1 clearly exhibits another population that is field-aligned (FAB) between 07:00 UT and 07:20 UT with a pitch angle $\alpha \sim 0°$. This is particularly evident for ion energy $\geq$2.4 keV (top 2 panels) as well as on Figure S3 in Supporting Information S1 which shows the ion velocity distributions in the $v_{\parallel} - v_{\perp}$ velocity plane. While the pick-up ion population is present during the entire time interval, the FAB sudden appearance coincides with a rapid IMF rotation occurring at 06:59:15 UT and making MAVEN magnetically connected to the shock as illustrated in Figure 2. On this latter figure, the top panel shows the angles θ_{BV} (in blue) and α_P (in red). The following two panels display the angles θ_{Bn} and θ_{Vn} that the local shock normal makes with the magnetic field direction and the solar wind velocity, respectively (Figure S2 in Supporting Information S1). These angles are calculated in the section of the bow shock to which MAVEN is connected. The third panel shows the distance *DIST* along the magnetic field line between MAVEN's position and the shock. These connection parameters are remotely calculated and their determination necessitates the use of a model for the Martian bow shock boundary. The shape of the bow shock of Mars has been extensively investigated using various satellite data sets. Statistical in nature, all models revolve around a fitting procedure that uses shock crossing locations to determine the best conic section (Schwingenschuh et al., 1990; Slavin et al., 1991; Trotignon et al., 1991; Vignes et al., 2000). With some exceptions (Ramstad et al., 2017), in all these models the conics' parameters are fixed and

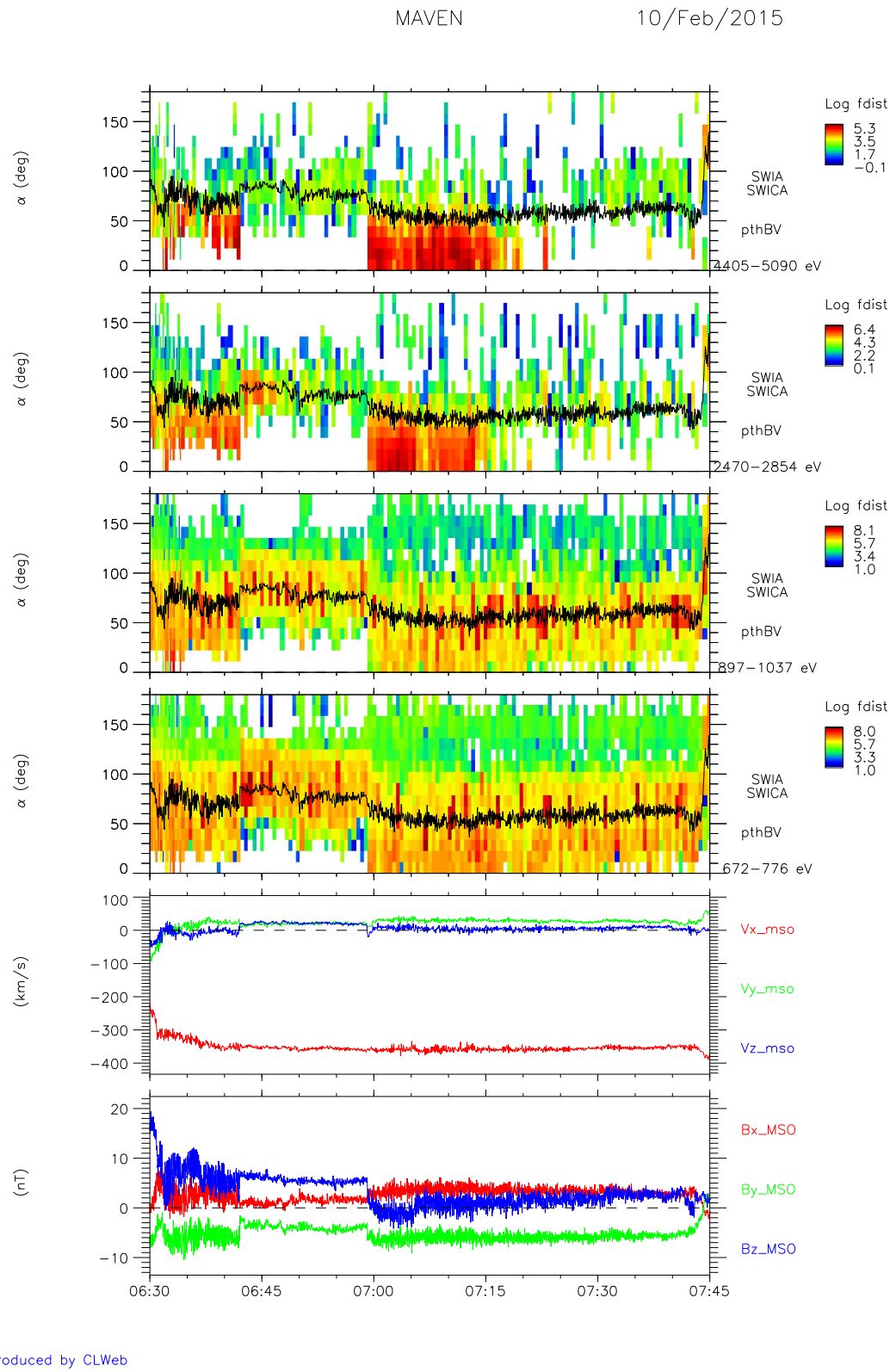

Figure 1. The four top panels respectively show the plasma rest frame ion pitch angle spectrograms from four selected energy ranges on 2015 February 10 during 06:00–07:45 UT time interval. The angle $\alpha_P = \pi - \theta_{BV}$ is shown in black trace superposed on each panel. The two bottom panels show the solar wind velocity and the magnetic field components in the Mars-centered Solar Orbital system of coordinates.

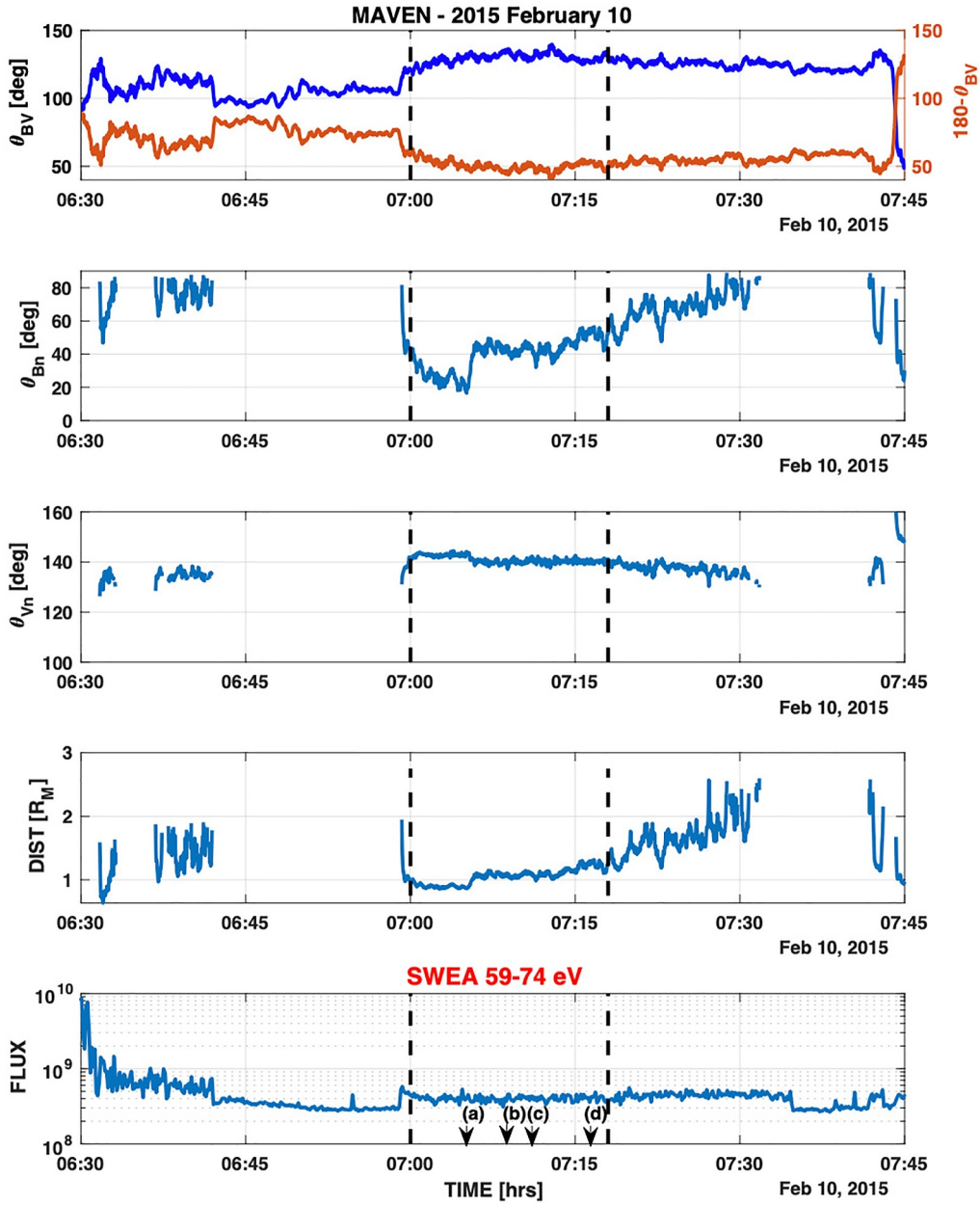

Figure 2. The angles θ_{BV}, α_P, θ_{Bn} and θ_{Vn} are shown in the top three panels respectively. The fourth panel shows the distance along the magnetic field direction between MAVEN's position and the bow shock while the bottom panel shows the $59 - 74$ eV energies electron differential flux which unit is $\left[\left(\text{cm}^2.\text{eV.str}\right)^{-1}\right]$ from SWEA instrument. The two vertical dashed lines indicate where the field-aligned beams are observed. The arrows at the bottom indicate the times corresponding to the velocity distributions shown in Figure 3.

no adjustment to solar wind and solar activity conditions are considered. For the present study, the nominal model of Vignes et al. (2000) is used, and as it is shown below, it provides satisfactory results. The connection parameters are calculated according to a conventional procedure. First, at a given time, the intersection point of the magnetic field line threading the spacecraft with the shock is determined. At the intersection point, the direction of the normal to shock is directly derived from the shock model. The angles θ_{Vn} and θ_{Bn} are therefore calculated using the solar wind and magnetic field (IMF) data. In addition, the distance *DIST* along the magnetic field direction between MAVEN's position and the intersection point, determined above, is computed. Prior to the

calculation, a smoothing operation employing the running average technique is applied to the three components of the IMF in order to mitigate the errors due to IMF fluctuations.

The bottom panel displays the differential flux of 59−74 eV energetic electrons measured by the SWEA detector. The choice of this energy is solely instructive, the same pattern is seen on all SWEA energy channels with 14 eV $\leq E \leq$ 1360 eV. Energetic electrons emanating from the shock and their flux level are always above those of the solar wind electrons at the same energy. These backstreaming electrons are observed under the condition of magnetic connection and consequently the energetic flux level forms an unambiguous proxy for the magnetic connection (Meziane et al., 2017). Figure 2 indeed indicates that the enhanced energetic electron flux simultaneously appears when the IMF line threading the spacecraft is connected to the shock. This model remarkably captures the short-lived abrupt energetic electron flux enhancement at 07:42:30 UT indicating that the shock has not moved significantly.

The sudden disappearance of the FAB population later than 07:20 UT is due to the fact that the magnetic field lines direction lies outside of the detector FOV. The observations of FABs coincide initially with a monotonic decrease of the shock θ_{Bn} reaching a minimum of 20° followed by a sequence in which θ_{Bn} gradually increases to an oblique configuration; during the entire interval, the θ_{Vn} angle remains nearly constant. The regular changes of θ_{Bn} angle prompt a characterization of the beam particle distribution, which will allow a more precise identification of the production mechanism of the observed beams. Overall, 26 FABs have been collected during the time interval shown on Figure 1, in which their properties including the density, the bulk speed and parallel thermal spread have been determined individually (see next section). Also, for each event, the corresponding θ_{Vn} and θ_{Bn} are determined according to the method described above.

During the orbit of MAVEN preceding the one examined above, other FAB events have been identified based on ion signatures in the pitch-angle spectrogram and the velocity distribution. The FABs collected during the same day between 02:25 UT and 04:00 UT are seen on IMF lines that connect the bow shock at various shock geometries. A cluster of 31 FABs has been selected, and their corresponding ion velocity distributions are studied. A sample of two-dimensional ion velocity distributions are shown in Figure S4 in Supporting Information S1. Finally, for each FAB event, the associated shock geometry (θ_{Vn} and θ_{Bn}) is determined according to the method described above.

2.4. Analysis of FAB Velocity Distributions

We now carry out a quantitative characterization of the observed beams. Figure 3 shows a sample of reduced parallel velocity ion distributions associated when FABs are observed. Four snapshots are selected and the corresponding times are indicated by vertical arrows at the bottom of Figure 3. In each panel, the blue dots represent the individual determination from SWICA of the distribution for each parallel speed while the green dots show the measurement from SWIFA. The distributions are represented in the solar wind frame of reference and obtained through the integration over $v_\perp$ of the two-dimensional distribution in the $v_\parallel - v_\perp$ space; the procedure implicitly assumes gyrotropic distributions.

Essentially, SWIFA spans over the thermal solar wind while SWICA measures the ion distribution over its entire FOV. Both SWICA and SWIFA capture the main distribution function maxima at $v_\parallel \sim 0$, corresponding to the peak of the solar wind distribution. However, the SWIFA thermal spread around the peak is more representative of what is expected for a solar wind temperature. Furthermore and at high energy, SWICA exhibits a secondary peak in the distribution function which corresponds to the FAB population. A Maxwellian function is used to fit the FAB population and the result is indicated by the red curve (Figure 3). Although the distribution peak is satisfactorily well fitted, it remains poor at high energy due to the presence of a significant tail in the FAB velocity distribution. For the bulk component of the distribution, the chi-square goodness of fit test indicates that the Maxwellian fit hypothesis to data is not rejected at 1% significance level. The beam speeds obtained correspond to the peak of the Maxwellian distribution fit.

The estimation of the FAB density n_B requires caution and it is calculated as follows. Assuming that the FAB parallel velocity distribution is fit by a Maxwellian for which f_{0B} is the distribution peak value, that is, $f(v_\parallel) = f_{0B} \exp\left(-(v_\parallel - v_B)^2/v_{Bth}^2\right)$, it is trivial to deduce that the FAB proton density is

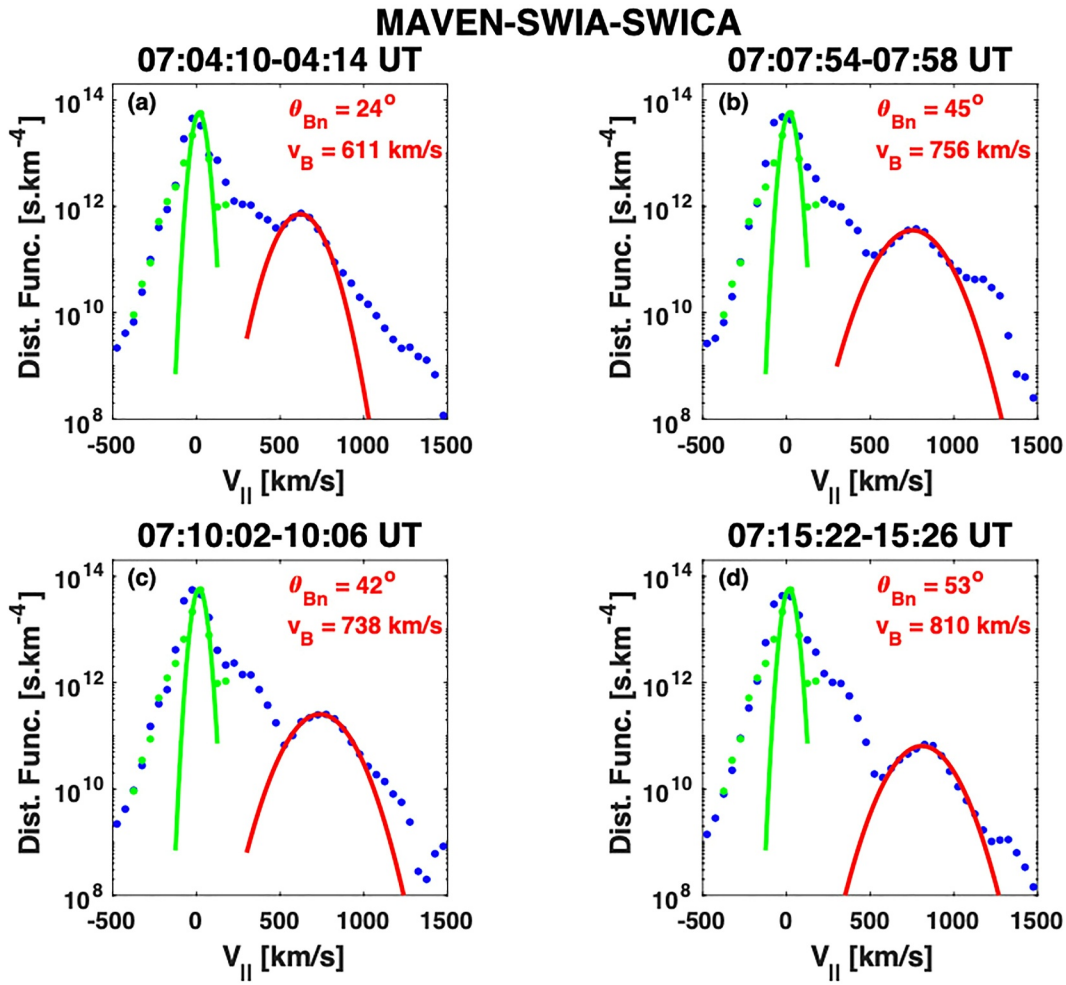

Figure 3. Snapshots of ion parallel velocity distribution collected by SWICA (blue dots) and SWIFA (green dots). The red (green) curve represents the best Maxwellian fit of the field-aligned beam (solar wind) component.

$$n_B = \frac{\sqrt{\pi}}{2} f_{0B} \times v_{Bth} \left[1 + erf\left(\frac{v_B}{v_{Bth}} \right) \right] \tag{3}$$

where $erf(x)$ represents the error function and v_{Bth} is the thermal parallel speed obtained from the Maxwellian fit. Equation 3 is obtained from the integration of $f(v_{\|})$ between 0 and infinity (Gradshteyn & Ryzhik, 2007). On one hand, Equation 3 may overestimate the beam density n_B as it assumes that the shock produces FAB with unrestricted $v_B \geq 0$ values; the premise is fully validated since only FAB protons with a parallel speed out running the shock speed can escape upstream. On the other hand, ignoring the FAB tail induces an underestimation in the evaluation of the beam density n_B. For each collected FAB, both the beam density and the parallel velocity are determined based on a Maxwellian fit. Figure 4 shows the obtained results for all the 57 beams collected during the two intervals. The left (right) panel shows the normalized beam speed v_B/V_{SW}(density ratio n_B/n_{SW}) versus the shock speed normalized to the solar wind speed. For both time intervals, $V_{SW} \sim 360$ km/s and $n_{SW} \sim 5.5$ cm^{-3}.

3. Production Mechanism

The association of FABs' energy with the bow shock geometry prompts a scrutiny of their production mechanism. The Terrestrial foreshock is the archetype of planetary foreshocks, and is therefore used as a reference. The production mechanism models developed for the terrestrial case can be employed for Mars. The strongest

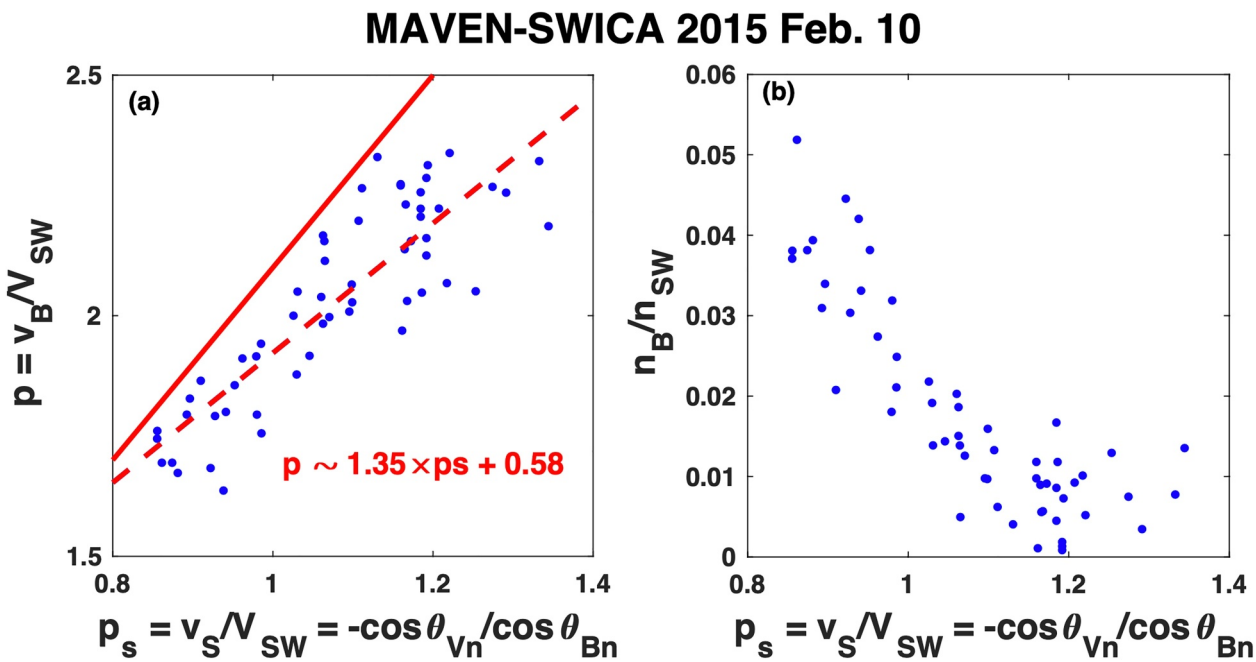

Figure 4. Each thick dot represents the normalized to the solar wind, the parallel beam velocity (left panel) and the beam density (right panel) versus the shock speed; the dashed red line indicates the best linear fit. The red straight line has a slope of 2.

evidence in support of ion reflection as the source for FABs is based upon energy conservation arguments (Paschmann et al., 1980; Schwartz et al., 1983). In this context, it also has been reported that the specular reflection of a portion of the solar wind accounts for backstreaming ion distributions seen in the quasi-parallel terrestrial foreshock (Gosling et al., 1982). This mechanism produces ion distributions that are field-aligned only for a parallel shock geometry $(\theta_{Bn} \sim 0)$. In addition, the post-encounter parallel ion velocity decreases when the shock θ_{Bn} increases. Consequently, the observations described in the previous section rule out specular reflection as the mechanism responsible for the production of FABs.

Another well known mechanism has been reported by Sonnerup (1969), namely that the reflection of a portion of the solar wind ions, which can occur as a quasi-adiabatic process, that is, the particle magnetic moment $\mu = v_{\perp}^2/B$ remains unchanged in the deHoffmann-Teller reference frame. The mechanism predicts a post encounter normalized parallel speed $p = v_B/V_{SW}$ given by (Meziane et al., 2004):

$$p = -(1+\delta)p_s \tag{4}$$

where $p_s = -\cos\theta_{Vn}/\cos\theta_{Bn}$ is the shock speed normalized to the solar wind speed (θ_{Vn} is obtuse while θ_{Bn} is acute) and $0 < \delta \leq 1$. The shock speed V_S emerges as deHoffman-Teller velocity in the solar wind reference frame. The adiabatic reflection occurs when $\delta = 1$. Previous FAB observations indicated that δ is in the range $0.85-1.0$ (Paschmann et al., 1980). From Figure 4, it is clear that the FAB beam speed consistently satisfies Equation [4] with a factor $\delta = 0.35 \pm 0.21$. When only FABs seen during the time interval from 06:30 to 07:45 UT are considered, the analysis provides a factor $\delta = 0.38 \pm 0.27$. For the 02:25–04:00 UT time interval, we found $\delta = 0.22 \pm 0.41$. In all cases, the Martian FABs speed appears significantly smaller than their terrestrial counterpart. The agreement with the reflection model indicates that the Martian FABs agree very well with the known characteristics of the terrestrial foreshock counterparts. In another mechanism, FABs may emerge as a portion of the ring distribution that had been strongly pitch angle scattered immediately after a specular reflection (Kucharek et al., 2004). Because that this process predicts a FAB normalized velocity $p = 2$, it follows a significant ion beam energy loss in order to account for the observations presented above.

Although the solar wind protons appear to provide the primary source for the FAB population, pickup protons could be also regarded as a plausible source due to their omnipresence. Following their generation, pick up ions

encounter the shock and are either directly transmitted downstream or accelerated before they are transmitted upstream or downstream, depending upon the geometry of their interaction with the shock (Lee et al., 1996). In a non-radial IMF direction, the pickup protons that are reflected have a significant velocity component perpendicularly to the magnetic field direction. This seems to rule out pickup protons as the population source for the FAB reported in the preset study.

4. Discussion

The presence of a field-aligned ion population in the upstream region of the Martian bow shock is now well established. The beams appear to emanate from a shock region where the IMF lines make an angle θ_{Bn} with the shock normal in the $19°-61°$ range. In the case of Earth, the source region extends to $\theta_{Bn} \sim 70°$. More studies are needed to validate whether or not the Martian upper region limit results from the restricted SWIA FOV. In addition, it seems that the FABs source region at Mars stretches to quasi-parallel region down to $\theta_{Bn} \sim 20°$. Terrestrial foreshock FABs are seldom seen at such a shock geometry and it is likely that uncertainties that result from the bow shock position do not account for the discrepancy. In the terrestrial foreshock, the critical θ_{Bn} at which FABs are observed is related to the angle θ_{BV} (Andrés et al., 2015; Meziane & d'Uston, 1998). Nevertheless, this critical angle is consistent with a quasi-perpendicular geometry. Again, additional studies are necessary to make precise the source region for quasi-parallel shock geometries.

This study provides the first detailed evidence of FAB velocity distributions inside the Martian foreshock, offering new insights into their production mechanisms. Qualitatively, the terrestrial and Martian foreshock beams share similar characteristics, including a Maxwellian core and a high-energy tail in their respective parallel velocity distribution functions (Meziane et al., 2007). As shown in Figure 4, the scaling of the parallel beam velocity relative to the shock speed suggests that a reflection process involving a portion of the solar wind is the primary mechanism driving the formation of the beams.

All FABs that are found have a speed that overtake the solar convection, fulfilling the escape upstream condition. The present findings seem to indicate that the Martian foreshock FABs tend to have slower speeds when compared to their terrestrial counterparts. Most notably, this difference in speed is not linked to variations in interplanetary conditions or/and the scale size of the bow shock surface. The behavior of the backstreaming electrons at Mars provides some useful context (Meziane et al., 2017).

Finally, the efficiency of the Martian bow shock in reflecting can be quantified using the FAB distribution. As shown on Figure 4b, the ratio of FAB density to solar wind density peaks at $\sim$5% with an average $\langle n_B/n_{SW} \rangle \sim 1.70\%$. The ratio is comparable to that observed in terrestrial foreshock FABs (Bonifazi & Moreno, 1981). The decrease in beam density with θ_{Bn} is expected, as fewer ions can escape upstream given a higher velocity threshold is required in such a geometry. Moreover, the parallel beam thermal width (not shown) appears to be weakly dependent upon the shock geometry. On average, we find the full width at half maximum $\sigma_{B\|} \sim 0.25 V_{SW}$, which is of the order value observed for terrestrial FABs $(\sim 0.23 V_{SW})$ (Meziane et al., 2013).

Data Availability Statement

The research described in this manuscript utilizes publicly available data from the MAVEN mission (https://pds-ppi.igpp.ucla.edu/mission/MAVEN), including data from the SWIA instrument (Halekas et al., 2015), MAG instrument (Connerney et al., 2015) and SWEA instrument (Mitchell et al., 2016).

Acknowledgments
K.M. thanks Emmanual Penou for his devotion in providing his valuable help in CL software development tool. Parts of this work for the observations obtained with the SWEA instrument are supported by the French space agency CNES (National Centre for Space Studies).

References

Andrés, N., Meziane, K., Mazelle, C., Bertucci, C., & Gómez, D. (2015). The ULF wave foreshock boundary: Cluster observations. *Journal of Geophysical Research: Space Physics*, *120*(6), 4181–4193. https://doi.org/10.1002/2014JA020783

Barabash, S., & Lundin, R. (1993). Reflected ions near Mars: PHOBOS-2 observations. *Geophysical Research Letters*, *20*(9), 787–790. https://doi.org/10.1029/93GL00834

Bonifazi, C., & Moreno, G. (1981). Reflected and diffuse ions backstreaming from the Earth's bow shock 1. Basic properties. *Journal of Geophysical Research*, *86*(A6), 4397–4404. https://doi.org/10.1029/JA086iA06p04397

Connerney, J. E. P., Espley, J., Lawton, P., Murphy, S., Odom, J., Oliversen, R., & Sheppard, D. (2015). The MAVEN magnetic field investigation. *Space Science Reviews*, *195*(1–4), 257–291. https://doi.org/10.1007/s11214-015-0169-4

Delva, M., Mazelle, C., & Bertucci, C. (2011). Upstream ion cyclotron waves at Venus and Mars. *Space Science Reviews*, *162*(1–4), 5–24. https://doi.org/10.1007/s11214-011-9828-2

Gosling, J. T., Thomsen, M. F., Bame, S. J., Feldman, W. C., Paschmann, G., & Sckopke, N. (1982). Evidence for specularly reflected ions upstream from the quasi-parallel bow shock. *Geophysical Research Letters*, *87*, 1333–1336. https://doi.org/10.1029/GL009i012p013334

Gradshteyn, I. S., & Ryzhik, I. M. (2007). *Table of integrals, series, and products*. Elsevier Academic Press.

Halekas, J. S., Taylor, E. R., Dalton, G., Johnson, G., Curtis, D. W., McFadden, J. P., et al. (2015). The solar wind ion analyzer for MAVEN. *Space Science Reviews*, *197*(1–4), 125–151. https://doi.org/10.1007/s11214-013-0029-z

Jakosky, B. M., Lin, R. P., Grebowsky, J. M., Luhmann, J. G., Mitchell, D. F., Beutelschies, G., et al. (2015). The Mars atmosphere and volatile evolution (MAVEN) mission. *Space Science Reviews*, *195*(1–4), 3–48. https://doi.org/10.1007/s11214-015-0139-x

Jarvinen, R., & Kallio, E. (2014). Energization of planetary pickup ions in the solar system. *Journal of Geophysical Research: Planets*, *119*(1), 219–236. https://doi.org/10.1002/2013JE004534

Kucharek, H., Möbius, E., Scholer, M., Mouikis, C., Kistler, L. M., Horbury, T., et al. (2004). On the origin of field-aligned beams at the quasi-perpendicular shock: Multi-spacecraft observations by Cluster. *Annales Geophysicae*, *22*, 2301–2308. https://doi.org/10.5194/angeo-22-2301-2004

Lee, M. A., Shapiro, V. D., & Sagdeev, R. Z. (1996). Pickup ion energization by shock surfing. *Journal of Geophysical Research*, *101*(A3), 4777–4789. https://doi.org/10.1029/95JA03570

Madanian, H., Omidi, N., Sibeck, D. G., Anderson, L., Ramstad, R., Xu, S., et al. (2023). Transient foreshock structures upstream of Mars: Implications of the small martian bow shock. *Geophysical Research Letters*, *50*(8), e2022GL101734. https://doi.org/10.1029/2022GL101734

Mazelle, C., Winteralter, D., Sauer, K., Trotignon, J. G., Acuña, M. H., Baumgärtel, K., et al. (2004). Bow shock and foreshock phenomena at Mars. *Space Science Reviews*, *111*(1), 115–181. https://doi.org/10.1029/95JA03570

Meziane, K., & d'Uston, C. (1998). A statistical study of the upstream intermediate ion boundary in the Earth's foreshock. *Annales Geophysicae*, *16*(2), 125–133. https://doi.org/10.1007/s00585-998-0125-7

Meziane, K., Hamza, A. M., Wilber, M., Mazelle, C., & Lee, M. A. (2013). On the field-aligned beam thermal energy. *Journal of Geophysical Research: Space Physics*, *118*(11), 6946–6954. https://doi.org/10.1002/2013ja019060

Meziane, K., Mazelle, C. X., Romanelli, N., Mitchell, D. L., Espley, J. R., Connerney, J. E. P., et al. (2017). Martian electron foreshock from MAVEN observations. *Journal of Geophysical Research: Space Physics*, *122*(2), 1531–1541. https://doi.org/10.1002/2016JA023282

Meziane, K., Wilber, M., Hamza, A. M., Mazelle, C., Parks, G. K., Rème, H., & Lucek, E. (2007). Evidence for a high energy tail associated with foreshock field-aligned beams. *Journal of Geophysical Research*, *112*(A1), A01101. https://doi.org/10.1029/2006JA011751

Meziane, K., Wilber, M., Mazelle, C., LeQuéau, D., Kucharek, H., Lucek, E., et al. (2004). Simultaneous observations of field-aligned beams and gyrating ions in the terrestrial foreshock. *Journal of Geophysical Research*, *109*(A5), A05107. https://doi.org/10.1029/2003JA010374

Mitchell, D. L., Mazelle, C. X., Sauvaud, J.-A., Thocaven, J.-J., Rouzaud, J., Fedorov, A., et al. (2016). Current carriers in the near-Earth cross-tail current sheet during substorm growth phase. *Space Science Reviews*, *200*(1–4), 495–528. https://doi.org/10.1007/s11214-015-0232-1

Paschmann, G., Sckopke, N., Asbridge, J. R., Bame, S. J., & Gosling, J. T. (1980). Energization of solar wind ions by reflection from the Earth's bow shock. *Journal of Geophysical Research*, *85*(A9), 4689–4693. https://doi.org/10.1029/JA085iA09p04689

Ramstad, R., Barabash, S., Yoshifumi, F., & Holmström, M. (2017). Solar wind- and EUV-dependent models for the shapes of the Martian plasma boundaries based on Mars Express measurements. *Journal of Geophysical Research: Space Physics*, *122*(7), 7279–7290. https://doi.org/10.1002/2017JA024098

Schwartz, S. J., Thomsen, M. F., & Gosling, J. T. (1983). Ions upstream of the Earth's bow shock: A theoretical comparison of alternative source populations. *Journal of Geophysical Research: Space Physics*, *88*(A3), 2039–2047. https://doi.org/10.1029/JA088iA03p02039

Schwingenschuh, K., Riedler, W., Lichtenegger, H., Yeroshenko, Y., Sauer, K., Luhmann, J. G., et al. (1990). Martian bow shock: Phobos observations. *Geophysical Research Letters*, *17*(6), 889–892. https://doi.org/10.1029/GL017i006p00889

Slavin, J. A., Schwingenschuh, K., Riedler, W., & Yeroshenko, Y. (1991). The solar wind interaction with Mars: Mariner 4, Mars 2, Mars 3, Mars 5 and PHOBOS 2 observations of bow shock position and shape. *Journal of Geophysical Research*, *96*(A7), 11235–11241. https://doi.org/10.1029/91JA00439

Sonnerup, B. U. O. (1969). Acceleration of particles reflected at a shock front. *Journal of Geophysical Research*, *74*(5), 1301–1304. https://doi.org/10.1029/JA074i005p01301

Thomsen, M. F. (1985). Upstream suprathermal ions. In R. G. Stone & B. T. Tsurutani (Eds.), *Collisionless shocks in the heliosphere: A tutorial review* (pp. 253–270).

Trotignon, J. G., Grard, R., & Klimov, S. (1991). Location of the Martian bow shock measurements by the plasma wave system on PHOBOS-2. *Geophysical Research Letters*, *18*(3), 365–368. https://doi.org/10.1029/91GL00025

Vignes, D., Mazelle, C. X., Rème, H., Acuña, M. H., Connerney, J. E. P., Lin, R. P., et al. (2000). Solar wind interaction with Mars: Locations and shapes of the bow shock and the magnetic pile-up boundary from the observations of the MAG/ER Experiment onboard Mars Global Surveyor. *Geophysical Research Letters*, *27*(1), 49–52. https://doi.org/10.1029/1999GL010703

Yamauchi, M., Futaana, Y., Fedorov, A., Frahm, R. A., Dubinin, E., Lundin, R., et al. (2012). Ion acceleration by multiple reflections at Martian bow shock. *Earth Planets and Space*, *64*(2), 61–71. https://doi.org/10.5047/eps.2011.07.007

Yoon, P. H., Ziebell, L. F., & Wu, C. S. (1991). Self-consistent pitch angle diffusion of newborn ions. *Journal of Geophysical Research*, *96*(A4), 5469–5478. https://doi.org/10.1029/90JA02756